Agric Res J ***62*** *(5): 578-594, October 2025*
DOI: 10.5958/2395-146X.2025.00065.2

SPATIOTEMPORAL ANALYSIS OF LAND USE AND LAND COVER CHANGES IN TOKWE SUBCATCHMENT, ZIMBABWE: IMPLICATIONS FOR AGRICULTURE

Josephine Mwafuka[1,2]* and Tirivashe P Masere[1]
[1]Department of Land and Water Resources Management, Midlands State University, P Bag 9055, Gweru, Zimbabwe
[2]Research, Innovation and Postgraduate Studies, Manicaland State University of Applied Sciences, Stair Guthrie Road, P Bag 7001, Fernhill, Mutare, Zimbabwe

www.IndianJournals.com
Not for Commercial Use
Downloaded From IP - 216.73.217.51 on dated 03-Nov-2026

ABSTRACT

The study integrated geospatial mapping and modeling techniques to detect, simulate, and predict land use land cover (LULC) dynamics in the Tokwe Sub Catchment, providing a comprehensive framework for understanding and managing land use changes. To simulate spatiotemporal dynamic transition potential LULC changes, a multi-temporal remotely sensed big data acquired from Landsat TM/OLI for the period 1998 to 2023 with a 5-year interval was utilized. The study further predicted LULC changes for the period 2023 to 2043. Dependent variables (classified LULC maps), independent variables (DEM, slope, and population density) and an integrated CA-ANN algorithm within the MOLUSCE plugin of QGIS were deployed. Support Vector Machine (SVM) classifiers in Arcmap 10.5 were also utilized. Robust ground truthing was conducted for accuracy assessment of LULC for 2023, historical Google Earth Pro images were utilized for 1998, 2003, 2008, 2013 and 2018, through the use of overall accuracy and kappa coefficient indices. It was observed that between 1998 and 2023, the area (%) under water body, mining, wetland, cultivation and bareland increased by 67.8%, 97,0%, 21.5%, 16.7% and 42.6% respectively, while commercial forest and natural forest decreased by -8.6% and -82.0% respectively. The kappa coefficients for 1998, 2003, 2008, 2013 and 2018 were 0.79, 0.75, 0.87 and 0.85 respectively. LULC changes were attributed to anthropogenic factors that include increase in population and agricultural activities. The projection for 2043 indicate that water bodies, wetland, cultivation and natural forest would increase by 63.4%, 71.2%, 74.7% and 21.0 % respectively, while commercial forest, bare land and mining are projected to drop by -13.8%, -43.8% and -10.9%, respectively. The study provides a continuous methodological framework for stakeholders, including Environmental Management Agency, policymakers, legislators, catchment councils, miners, and farmers, thereby enabling the integration of geospatial technologies into environmental management practices for sustainable resource use and catchment resilience.

Keywords: Catchment management, LULC changes, LULC prediction, Tokwe Subcatchment

Agricultural expansion and rapid urbanization are the main drivers of land use and land cover (LULC) changes, causing extensive environmental impacts across different regions and time periods (Nut *et al.,* 2021; Renaud *et al.,* 2021). Such LULC modifications, particularly within catchments and sub-catchments, significantly impact surrounding ecosystems, including hydrological process, disrupt local livelihoods and pose challenges to effective environmental management (Mangi *et al.,* 2021; Mfwango *et al.,* 2022). With growing concerns over these impacts, Geographic Information Systems and Remote Sensing (GIS and RS) are valuable and widely recognized tools for monitoring, assessing and managing sub catchments. Thus, LULC maps that are GIS-aided are critical in catchment studies as they directly indicate hydrological setups, making them indispensable for accurately assessing watershed behavior, predicting environmental impacts and guiding sustainable land and water resource management.

Various studies integrating GIS and RS in watershed and catchment research employing the Soil Water Analysis Tool (SWAT) modeling in Germany, combining geospatial techniques with Revised Universal Soil Loss Equation (RUSLE) in Cambodia's Stung Sangkae Catchment and LULC classification in Poland's Western Carpathians have

*Corresponding author: josiengirazi@gmail.com
Date of receipt: 10.12.2024, Date of acceptance: 18.10.2025

yielded significant and informative results through advanced spatial analysis and modeling techniques (Nut *et al.,* 2021; Shukla *et al.,* 2023; Bucała-Hrabia, 2024). The studies highlight the power of geospatial technologies in environmental management, including at the sub-catchment level, yet their integration remains underutilized and not widely recognized in many developing nations. Developing countries like India have employed geospatial technologies to assess environmental impacts in the Upper Tapi River Sub-Basin where studies on LULC changes from 1975 to 2016 revealed an 18% increase in agricultural land, alongside a 7% and 10% decrease in forest and rangeland, respectively (Munoth and Goyal, 2020).

In China, spatiotemporal analysis of LULC changes using GIS, RS with supervised maximum likelihood classification and landscape metrics in the Lake Dianchi watershed (Yunnan-Guizhou Plateau) from 1974 to 2008 revealed distinct patterns with agricultural land showing significant spatial distribution shifts, forest land remained relatively stable at 22-26%, with only a 2.8% change, while wild grassland significantly declined from 18.8% to 7.1%, with a 62.1% loss (approximately 331.4 km²) (Zhao *et al.,* 2012). Although several developing countries have made compelling efforts to integrate GIS and remote sensing technologies in watershed and sub-catchment studies, Zimbabwe still shows limited research, application and utilization of these tools in environmental management and planning.

GIS-aided studies in Zimbabwe are limited despite being critical for understanding LULC changes which are essential for addressing environmental challenges that significantly alter subcatchment landscapes. To address this gap while promoting environmental sustainability and informed decision-making in subcatchment management, the study aims to integrate advanced GIS and RS techniques for the analysis of LULC changes and their impacts in Tokwe subcatchment utilizing the Support Vector Machine (SVM) classifier as it is one of the most powerful machine learning models useful in satellite image processing and supervised classification methods. The SVM classification has a higher accuracy in comparison to other algorithms, such as Random Forest (RF) and Maximum Likelihood (ML) classification (Basheer *et al.,* 2022). Further, using SVM classification for image classification ensures effective handling of high-dimensional data such as remotely sensed images. Despite its advantages, there is limited research that has used SVM and multi-layer perceptron - artificial neural network (MLP-ANN) based Cellular Automata (CA) technique in QGIS to accurately analyze LULC changes in Tokwe Subcatchment.

While there are studies that utilise either SVM or MLP-ANN for LULC classification, a significant gap exists in the comprehensive integration of both techniques with Cellular Automata (CA) models for predicting LULC changes in Zimbabwe's subcatchments. Current frameworks often rely on individual models, failing to exploit the synergies between SVM's robust classification capabilities and MLP-ANN's adaptability, when combined with CA's spatial and temporal dynamics. To provide explicit and critical findings that are science-based, the study incorporates socio-economic, environmental, and cultural factors that influence LULC changes in the Tokwe Subcatchment. This is to provide a tailored model that incorporates local data and ground-truthing efforts to improve the accuracy and reliability of predictions. Therefore, the research aims to integrate both techniques to understand the intricate complexities of LULC dynamics in Tokwe Subcatchment through incorporating SVM and MLP-ANN within a CA framework. This presents an opportunity to model, not only current conditions, but also future scenarios by simulating various LULC change scenarios. The strength of integrating these techniques overrides other models that rely on static datasets. The study provides a continuous methodological framework for various stakeholders, including the Zimbabwe National Water Authority (ZINWA), Environmental Management Agency (EMA), policymakers, legislators, catchment councils, miners, communities, and farmers, enabling the integration of geospatial technologies into environmental management practices for sustainable resource use and catchment resilience.

Theoretical Framework for LULC Change

The dynamics of LULC changes in Zimbabwe is comprehensively understood through the integration of frameworks: Political Ecology, Demographic and Land Use, and Socio-Ecological Systems (SES) (Fig. 1). Political Ecology emphasises how power relations, governance structures, and policy decisions shape resource access and environmental outcomes. The Fast-Track Land Reform Program (FTLRP) served as a critical example of how political agendas and land redistribution policies have dramatically transformed land ownership patterns and consequently altered land use. Complementing this, Demographic and Land

www.IndianJournals.com
Not for Commercial Use
Downloaded From IP - 216.73.217.51 on dated 03-Nov-2026

Use frameworks elucidate how population growth, migration, and resettlement associated with the FTLRP have intensified pressure on land resources, driving agricultural expansion, deforestation, and settlement proliferation. Meanwhile, the SES framework situates these changes within complex adaptive systems where social and ecological components interact, highlighting feedback loops between human livelihoods, ecosystem services, and environmental resilience. The framework demonstrates that LULC changes in Zimbabwe are deeply intertwined with political contestations, demographic shifts, and ecological processes, emphasising the need for integrated policies that address social equity, environmental sustainability, and land governance.

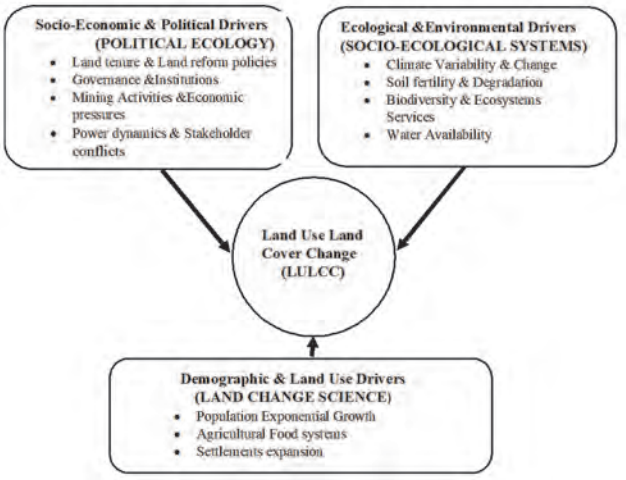


Fig. 1. Theoretical Framework for LULCC dynamics in Zimbabwe

The study is guided by the following research objectives: (i) the need to assess LULC changes at constant five-year intervals to understand LULC fluctuations that are often overlooked (ii) limited knowledge on the application of predictive models for future LULC changes in Tokwe Subcatchment (iii) limited information on the implications of LULC changes on reservoir sedimentation in Tokwe Subcatchment. To address the gaps, the study aimed to assess LULC change at five-year intervals (1998, 2003, 2008, 2013, 2018 and 2023) and to predict LULC changes for 2033 and 2043 in Tokwe Subcatchment. Finally, the study sought to understand the implications of LULC changes in the Tokwe Subcatchment on the sedimentation of Tugwi Mukosi Dam. By providing insights into LULC dynamics and their impacts, the study contributes to informed decision making and the development of sustainable catchment management practices.

MATERIALS AND METHODS

Study site description

Tokwe Subcatchment is situated in the south-eastern part of Zimbabwe. According to the hydrological demarcations, the Tokwe Subcatchment is one of the five major Subcatchments in Runde Catchment (Fig. 2). The physical characterisation of the area is defined by mean annual rainfall, received between November and April, which ranges from 458 mm to 660 mm with an average temperature of 20°C (Dzirekwa *et al.,* 2023). Dzirekwa *et al.* (2023) further indicate that Tokwe Subcatchment has mainly chromic luvisols with isolated patches of calcific fluvisols soils.

On the socio-economic dimension, Tokwe Subcatchment has national and regional importance because it has several reservoirs (Tugwi-Mukosi, Mushandike and Muzhwi). The reservoirs are critical for water supply, supporting various activities that include irrigation of sugar plantations, municipality water supply, fisheries, hydroelectric generation and recreational purposes. Further, the area is characterised by predominant asbestos mining at Mashava along the Great Dyke, culminating in substantial land degradation (Tonderai *et al.,* 2013). There are overcrowded communal areas in Tokwe Subcatchment where farmers mostly depend on dryland farming for their livelihoods (Mutowo and Chikodzi, 2013). The dams play a vital role in supporting the Lowveld sugarcane industry, which significantly contributes to Zimbabwe's economy. In addition, the Tokwe Subcatchment supports irrigation schemes like the Mushandike Irrigation Scheme, which are important for agriculture in the area (Malanco *et al.,* 2018). Demographically, Tokwe Subcatchment has 74,066 people. Of the total population, there are more females (54.01%) than males (45.99%) (Government of Zimbabwe, 2022 & 2023). There is uneven population density distribution of 47 people per km^2, where the population is concentrated around service centres and business centres like Ngundu, Chibi Turnoff, and Chivi District Service Centres.

Image pre-processing

A methodology framework was developed to analyse the performance and viability of the SVM classification method. Landsat images in radiance were converted to Top of Atmosphere (TOA) Reflectance (combined surface and atmospheric reflectance) in order to reduce the in between-

www.IndianJournals.com
Not for Commercial Use
Downloaded From IP - 216.73.217.51 on dated 03-Nov-2026

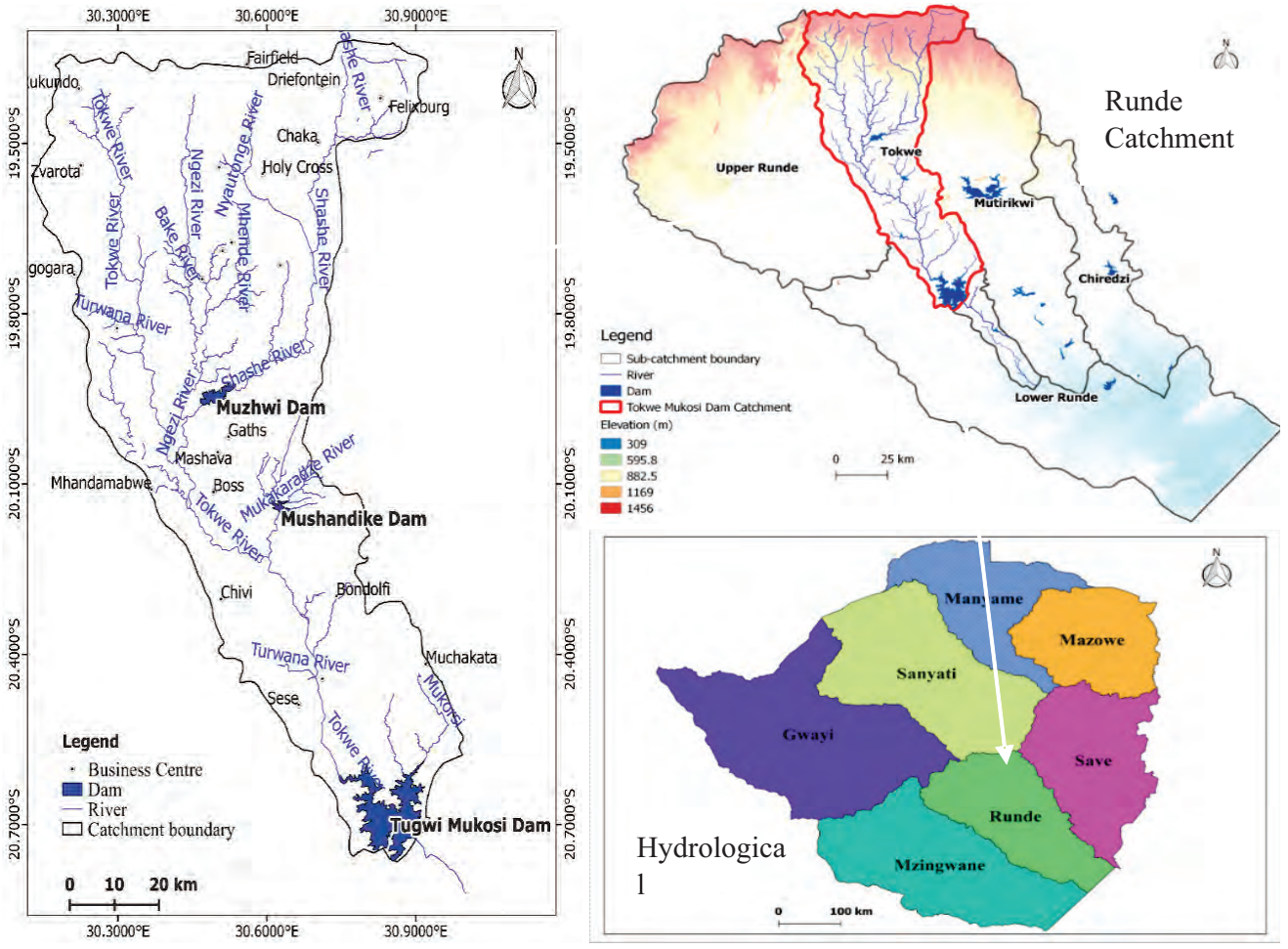


Fig. 2. Map of Tokwe Subcatchment

scene variability through a normalisation for solar irradiance. Utilising the raster calculator, radiometric correction is a technique for improving the brightness magnitude of a satellite image for better visibility and analysis (Haque and Basak, 2017). Landsat Satellite sensors capture land cover images as Digital Numbers (DNs) value rather than TOA reflectance. By adjusting the bias and gain levels for each band, radiometric correction was used to translate DNs into Top of Atmosphere (TOA) radiance measurements in Arcmap 10.5. The radiance data were converted to TOA reflectance using irradiance values at the sensor (Seyam *et al.,* 2023). This TOA reflectance (ρp), which is the unitless ratio of reflected versus

Table 1. Satellite data utilized in the study

Acquisition date	Satellite platform	Sensor name	Scene (Path / row)	Ground sample distance (Spatial resolution)	Source
27 July 2023	Landsat 8	OLI/TIRS	169/73	30*30 m	USGS
16 August 2018	Landsat 8	OLI/TIRS	169/74	30*30 m	USGS
29 September 2013	Landsat 8	OLI/TIRS	170/73	30*30 m	USGS
03 September 2013	Landsat 8	OLI/TIRS	170/74	30*30 m	USGS
20 August 2008	Landsat 4-5	TM	170/73	30*30 m	USGS
27August 2008	Landsat 4-5	TM	170/74	30*30 m	USGS
11September 2003	Landsat 4-5	TM	169/74	30*30 m	USGS
10 September 1998	Landsat 4-5	TM	169/73	30*30 m	USGS

www.IndianJournals.com
Not for Commercial Use
Downloaded From IP - 216.73.217.51 on dated 03-Nov-2026

total power energy (NASA, 2011), is calculated by:

$\rho p = (\pi * L\lambda * d2)/(ESUN\lambda * cos\theta s)$ where:

• $L\lambda$ = Spectral radiance at the sensor's aperture (at-satellite radiance)

d = Earth-Sun distance in astronomical units

• $ESUN\lambda$ = Mean solar exo-atmospheric irradiances

• θs = Solar zenith angle in degrees, which is equal to θs = 90° - θe where θe is the Sun elevation. It is fundamental pointing out that Landsat images are provided with band-specific rescaling factors that allow for the direct conversion from DN to TOA reflectance.

Image processing

Further, geometric correction of Landsat images involved spatially projecting the image dataset to WGS 1984-UTM Zone 36S. Subsequently, layer stacking, mosaicking, creation of composite images and sub-setting for image classification was done. Image enhancement through the histogram equalisation technique was performed. Histogram equalisation helps distinguish different features that might have the same colour but are sharply different in tone or brightness (Anteneh, 2022). Further, the sensitivity of red-edge to chlorophyll content extend a significant utility for LULC analysis (Sánchez-Espinosa and Schröder, 2019). Figure 3 shows the methodological framework for LULC classification using SVM classifiers in Arcmap 10.5.

Generation of training and test samples

A pixel-based supervised classification technique was employed for the LULC change classification of satellite images. Judicious analysis of the study area resulted in seven different land use classes being identified as shown in table 2. Based on these LULC classes, training samples were generated using defined polygons upon the various locations of different land use classes. The optimal spectral signature helped to reduce misclassification among mapped land uses (Griffel *et al.*, 2020).

The process of defining training samples involved the use of a stratified sampling technique. The collected training samples were grouped based on land cover. The extracted sampling points were split into 70% training and 30% validation samples using a stratified random sampling technique. Base map imagery from Arcmap 10.5 was used to visually evaluate high-resolution images from 2013, 2018, and 2023. A minimum of ten and a maximum of

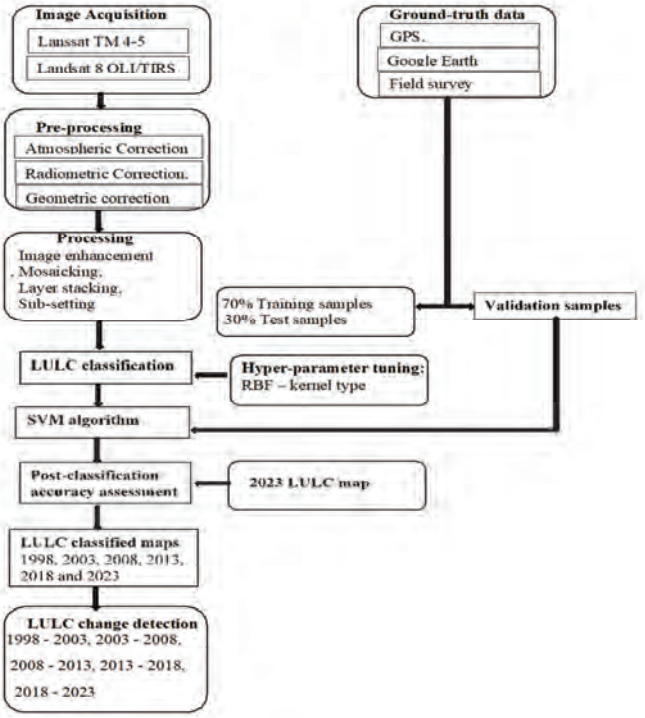


Fig. 3. Methodological framework for LULC classification based on SVM model

twenty-five training samples were assigned for each of the seven land use classes considered for image classification. The training shape file was then created as the training dataset for supervised classification.

Support Vector Machine Image Classification Algorithm

The LULC change analysis was conducted based on the SVM algorithm. Using a feature vector and model parameters, the SVM sought to identify the best hyperplane that defines the class boundary during the training phase. Only samples in the margin between classes were utilised to create the optimum

Table 2. Detailed description of Land Use Land Cover classes

LULC Types	LULC description
Water	Dams, reservoirs, ponds and rivers
Commercial forest	Intensively managed timber producing areas
Natural Forest	Naturally growing vegetation species
Cultivated land	Subsistence dominated cropped land
Bareland	Surfaces with no vegetation and rocky mountainous areas
Wetlands	Permanently waterlogged areas
Mining	Degraded mined areas devoid of tree cover

www.IndianJournals.com
Not for Commercial Use
Downloaded From IP - 216.73.217.51 on dated 03-Nov-2026

hyperplane in the SVM, and they are referred to as support vectors (Li *et al.,* 2019). In this study, the hyperparameter tuning strategy was employed to optimize the performance of SVM machine learning model for LULC classification. The thrust was to enhance the accuracy of the model and achieve credible results on the test dataset.

SVMs have different kernel types and parameters to improve accuracy and efficiency. The SVM's performance is dependent on the selection of the kernel type and in this study a Radial Basis Function (RBF) kernel was selected as it was found to be more suitable for LULC applications (Petropoulos *et al.,* 2010). The RBF kernel with a parameter value of 0.1 was employed. The regularisation parameter (C) was set to 100 to control the trade-off between maximising the margin and minimising the classification error. Each training sample pixel was assigned to a LULC class based on supplementary data derived from Google Earth images from each year of the study (Zhong *et al.*, 2021). SVM classification was then utilised for model training and the subsequent raster classification. Conversion of raster to polygon and eventually dissolving the vector polygon by grid code to create vector-based polygons of the seven LULC classes constituted a critical step. The area for each class was computed in square kilometres to facilitate area change detection in MS Excel 2016.

To avoid the subjectivity of manual point selection, the ArcGIS points-creating tool was used to generate random point layers for accuracy assessment (Chaaban *et al.,* 2022). In total, five hundred random points were created and distributed proportionally in relative classes. Classes with bigger areas such as crop cultivation and natural forest had more points than other classes with smaller areas. By overlaying the random points layer on the pre-processed satellite images, segments covering those points were distinguished based on ground truthing data and assigned to relative classes. To compute the accuracy of the classified thematic maps, ArcGIS's create assessment points tool was utilized to generate the table automatically, based on five hundred reference data sample points developed using random sampling on the classified image. As a rule, every classification class should have a minimum of fifty training samples (Shang *et al.,* 2018). Subsequently, the random points table was converted to KML format compatible with Google Earth Pro for validation (ground-truthing) of the seven LULC classes. Google Earth Pro images were observed and cross-referenced to determine the ground-truthing of the selected sample points. Each point position was analysed based on the polygon into which it was placed and compared to the reference image to determine whether it was accurately identified. These sample points were then converted into a confusion matrix. The confusion matrix was used to determine the kappa coefficient overall accuracies, including user and producer accuracies (Nedd, 2021). A series of reconnaissance field surveys were conducted for ground truthing data collection in 2023. Ground truthing data was recorded using a hand-held Garmin Global Positioning System (GPS) receiver so that the controlling points could easily be identified and used in the image validation process.

Post Classification and Accuracy Assessment

An ideal procedure in LULC analysis focuses on the assessment of classification accuracy before change detection and future prediction (Wang *et al.,* 2021) to test the precision and accuracy of classified imagery. Image classification performance was evaluated using the accuracy assessment tool in Arcmap 10.5 (Dey *et al.,* 2021) through randomly sampled ground truthing data. Overall accuracy (OA), user accuracy (UA), producer accuracy (PA), and kappa coefficient (Kappa) were calculated using Equations (1) to (4) based on the confusion matrix (Kafy *et al.,* 2021). Table 3 shows the Kappa coefficient intervals.

The model validation process of 500 reference points for each time frame (1998, 2003, 2008, 2013, 2018 and 2023) of the referenced data (regions of interests) was obtained using Google Earth Pro. These sample training points were randomly divided into training and test datasets in the proportion of 70 % (350 points) and 30% (150 points) respectively. The model validation process was supplemented by 212 actual field-level GPS reconnaissance points.

Table 3. Kappa coefficient intervals and its interpretation

K value	Strength of agreement
< 0	No agreement
0.00 - 0.20	Slight
0.20 - 0.40	Poor
0.40 - 0.60	Moderate
0.60 - 0.80	Substantial
0.80 - 1.00	Perfect agreement

Source: (Wang *et al.,* 2021)

www.IndianJournals.com
Not for Commercial Use
Downloaded From IP - 216.73.217.51 on dated 03-Nov-2026

$$OA = \sum_{i=1}^{r} \frac{Dii}{N} \quad (1)$$

$$UA = \frac{\sum D_{ij}}{X_{+i}} \quad (2)$$

$$PA = \frac{\sum D_{ij}}{X_{i+}} \quad (3)$$

$$Kappa = \frac{N\sum_{i=1}^{r} X_{ii} - \sum_{i=1}^{r} (X_{i+} * X_{+i})}{N^2 - \sum_{i=1}^{r} (X_{i+} * X_{+i})} \quad (4)$$

where, D_i is the number of correctly classified pixels,

- D_{ii} is the number of correctly classified pixels in row i,
- D_{ij} is the number of correctly classified pixels in column j,
- r is the number of rows in the matrix;
- X_{ii} is the number of pixels in row i and column i;
- X_{i+} and X_{+i} are the marginal totals of row i and column i respectively; and
- N is the total number of pixels (observations).

The producer's accuracy is related to omission error, the probability that a reference pixel is correctly classified. The user's accuracy represents the commission error, the probability that a pixel classified on the image is actually that land use on the ground (Foody, 2008). The kappa coefficient calculates the error generated by the classification process compared with an error of a completely random classification (Ruuska, 2018).

Modules for Land-Use Change Simulation (MOLUSCE) Interface in QGIS

MOLUSCE is a plugin in QGIS that functions similarly to the spatial analyst tool in Arcmap 10.5 (Guidigan *et al.,* 2019). It provides robust capabilities for analysing spatiotemporal dimensions in the LULC domain (Ragini *et al.,* 2023). MOLUSCE offers a user-friendly graphical user interface (GUI) composed of seven main components: Inputs, Evaluation Correlation, Area Change, Transition Potential Matrix, Cellular Automata Simulation, Validation, and Message (Al-Rubkhi *et al.,* 2017). In the initial step, the dependent and independent variables are prerequisite in constructing the model. Variables like DEM, slope, population density were considered as dependent while the independent variables include the LULC maps for times: T_1 and T_2. Within the MOLUSCE module, computational intelligence elements such as artificial neural networks (ANN) are utilised (Al-Rubkhi *et al.,* 2017). This includes three critical outputs: the Transition Potential map, the Sensitivity analysis, and the simulated LULC maps. The transition potential, calculated using the CA-ANN method, generates a probability matrix that serves as the basis for predicting future LULC changes (Zhang, 2022) (Fig. 4). The map of 2018 was used to simulate the LULC scenario for 2023 using MOLUSCE available in QGIS 3.40 software. Subsequently, the 2023 LULC map was utilised as a baseline map for prediction future 2033 and 2043 LULC maps.

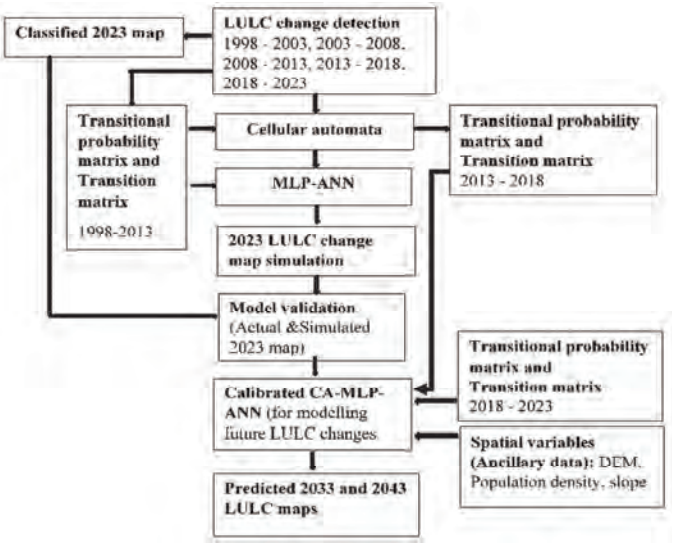


Fig. 4. Framework for LULC prediction process

In predicting the LULC maps, the following parameters were established: neighbourhood size = 1, iterations = 1000, hidden layers = 10, momentum = 0, and learning rate = 0.001. These parameters reflect assumptions about the model's structure and the learning process, influencing the accuracy and reliability of the predictions. Specifically, the choice of hidden layers and learning rate affects how well the ANN learn from the input data, while the number of iterations determines the extent of training the model undergoes before generating predictions categories.

Table 4. ANN variables for LULC Simulation process

Parameter	Value
Neighbourhood	3 × 3 pixel
Learning rate	0.01
Momentum	0.001
Hidden layers	10
Maximum iterations	1000

www.IndianJournals.com
Not for Commercial Use
Downloaded From IP - 216.73.217.51 on dated 03-Nov-2026

www.IndianJournals.com
Not for Commercial Use
Downloaded From IP - 216.73.217.51 on dated 03-Nov-2026

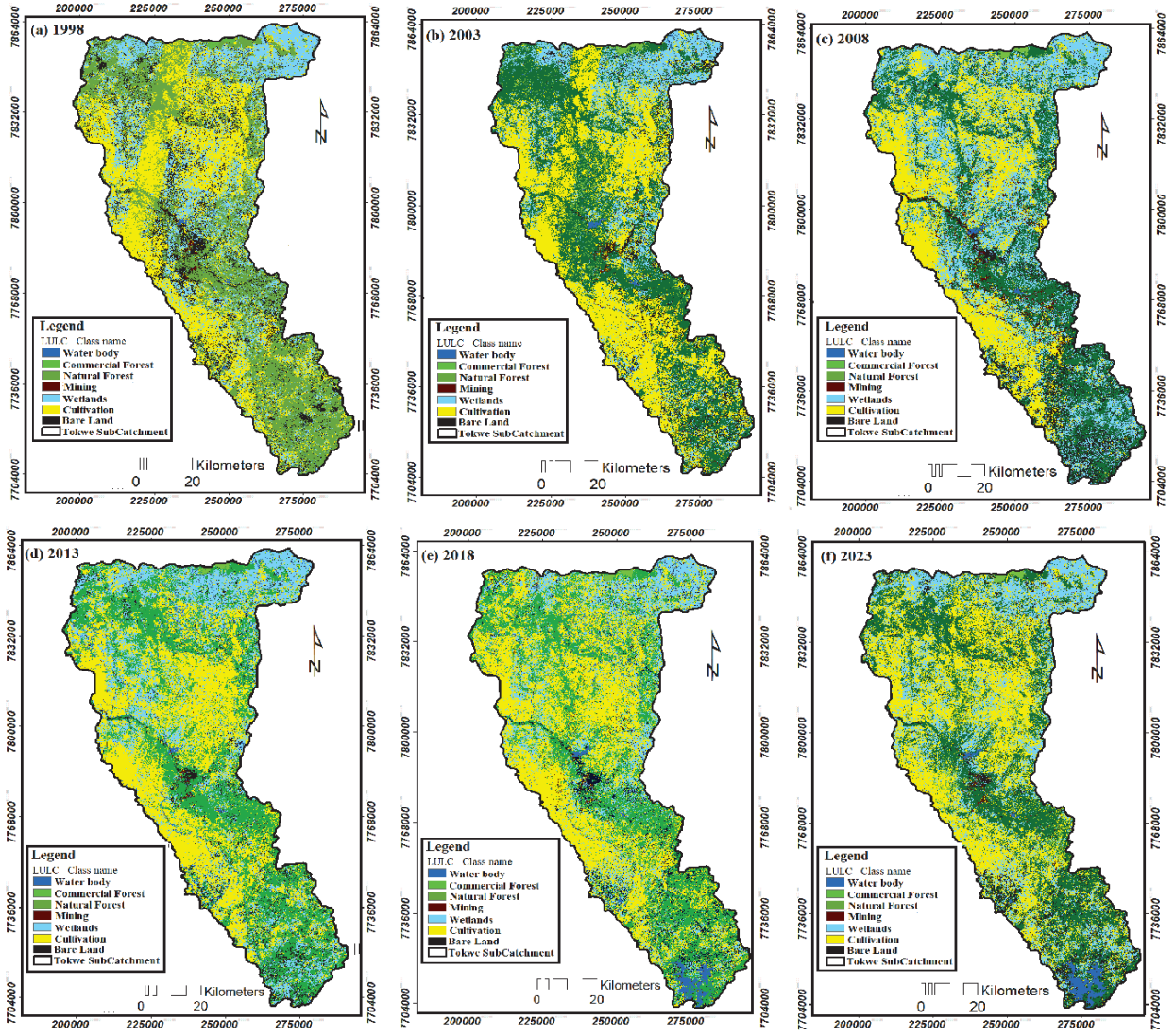


Fig. 5. SVM classification for years: (a) 1998, (b) 2003, (c) 2008, (d) 2013, (e) 2018 and (f) 2023

RESULTS AND DISCUSSION

Dynamics of LULC: 1998 to 2023

LULC change analysis was conducted and the image classification at 5-year intervals from 1998 to 2023 is illustrated in fig. 5

Dynamics of LULC between 1998 and 2023

The study area experienced drastic changes (Table 5) in LULC that jeopardises environmental sustainability where the dynamic fluctuations are visible at 5 year interval from 1998 to 2023. However, based on overall changes, there was an increase in the area (%) under water body, mining (artisanal and small scale), wetland, cultivation and bare land by 67.8%, 97.0%, 21.5%, 16.7% and 42.6% respectively. The increase in the water body and wetland was attributed to the Tugwi Mukosi Dam construction and subsequent water accumulation. The water body experienced a significant overall change from 1998 to 2023 which is 67.8% increase and this modification is perceived as normal. This was attributed to the fact that currently, Zimbabwe is experiencing significant climate variability, marked by frequent cyclones and extreme flooding weather events, which may contribute to unusually high-rainfall discharge. Literature indicates that Zimbabwe has experienced numerous flood disasters, particularly during the 2014-2017 floods and again in 2019, highlighting the country's vulnerability to extreme hydrological events (Mugambiwa and Makhubele, 2021). This was because the dominant factors influencing the variability of precipitation vary within season Inter Tropical Convergence Zone, La Nina episodes, Cyclones culminating in summer season rainfall in

Table 5. Land Use and Land Cover (LULC) area change

Area change (km^2)	1998	2003	5-year LULC changes	2008	2013	5-year LULC changes	2018	2023	Overall change	Overall %ge change
Water Body	25.4	59.1	33.7	44.2	131.4	87.2	196.4	132.6	107.2	67.8
Commercial Forest	134.5	198.3	63.8	165.5	146.8	-18.7	74.3	113.3	-21.2	-8.6
Natural Forest	2684.6	1069.5	-1615.1	932.3	724.2	-208.1	466.3	265.8	-2418.8	-82.0
Mining	41.1	1314.2	1273.1	2003.1	2521.3	518.2	2621.3	2653.3	2612.3	97.0
Wetlands	1658.1	2421.2	763.1	1074.7	1824.3	749.6	2250.4	2566.0	907.8	21.5
Cultivation	1323.5	2448.5	1124.9	1411.1	2058.1	647.0	2368.2	1854.1	530.6	16.7
Bareland	931.4	1541.1	609.7	1148.3	1470.4	322.1	1315.1	2311.2	1379.8	42.6

www.IndianJournals.com
Not for Commercial Use
Downloaded From IP - 216.73.217.51 on dated 03-Nov-2026

Zimbabwe. Between October and December, usually regarded as early summer, the atmosphere has a distinct extra-tropical nature with frequent cut-off lows while during the late summer period (January-March) tropical circulation systems are much more prevalent over Southern Africa (Dyson and Van Heerden, 2002; Manatsa and Reason, 2016).

Commercial forest and natural forest area were greatly depleted by -8.6% and -82.0%, respectively. The decline in natural forest area was attributed to the Fast-Track Land Reform Programme that began in 2000. The Fast-Track Land Reform Programme entailed resettling farmers and massive land clearing to pave the way for farming activities. The findings are in line with those of Sibanda and Tsuyuki (2022) who found that forest area declined from 1989 to 2020 in Hurugwe District, Zimbabwe. Sibanda and Tsuyuki (2022) analysed LULC using remote sensing and GIS techniques that assumed consistent data quality and direct attribution of land cover changes to human activities. In addition, the study established that natural forests were depleted and this was attributed to rural communities' heavy reliance on the forest for firewood and livelihood activities. Maviza and Ahmed (2020) attributed natural forest depletion to increased human activities such as artisanal and small-scale gold mining activities. In addition, climate change could be further negatively affecting farming activities (crop cultivation and natural forest area) due to low and erratic rainfall as well as high temperatures (Ndlovu *et al.,* 2020).

Bareland and mining area increased while the area under agricultural activities reduced during the study period. Increased bareland area meant that the soil would be exposed to rainfall splash effects thereby increasing its erodibility and subsequently implying an increase in reservoir sediment accumulation. The increase in bareland could be attributed to land degradation resulting from mining activities. The artisanal and small-scale mining (ASM) activities are mostly associated with unsustainable mining practices. This is because during mining activities there is rampant destruction of trees and mining pits are rarely reclaimed post mining activities (Ofosu *et al.*, 2020). Thus, environmental degradation is experienced, which results in increased reservoir sedimentation due to increased soil erosion.

The natural forest is a very important source of firewood and some livelihood activities that include indigenous fruits gathering, grazing area for livestock and apiary activities. Therefore, the depletion of natural forests would further increase the risk of poverty and environmental degradation, resulting in reduced agricultural productivity. Therefore, it is imperative to engage in sustainable mining practices and reforestation to enhance livelihood activities and mitigate environmental degradation as a means for addressing SDGs 1 (no poverty) and 15 (promoting sustainability of the environment).

Table 6. Confusion matrix during different years

Year	Overall accuracy	Kappa coefficient
1998	0.97	0.86
2003	0.96	0.84
2008	0.98	0.82
2013	0.88	0.83
2018	0.84	0.81
2023	0.95	0.91

SVM model validation of LULC

The confusion matrix shows high accuracy of classification in assessing LULC change. It compared the predicted LULC classes against the actual

observed classes. Kappa coefficient ranged from 0.81 to 0.91 for the years 1998 to 2023 (Table 6) and it is an indication of high reliability and accuracy of the classification model.

LULC transition potential modelling

Transitional potential modelling was used to analyse and predict the likelihood of LULC classes transitioning from one state to another over time often in the context of Markov chain. Rows of the matrix table represent the categories in the initial year, while the columns denote the same order of LULC categories in the final year. Class entries on diagonal represent the size of class stability, and each off-diagonal entry represents the size of the transition from one class to different classes. Essentially, values close to unity in diagonal entries represent the stability of a category. Researchers mostly use transition matrices to compare the temporal changes in different regions (Xiao *et al.*, 2021). An illustration on how each LULC type was projected to change in the study area during the periods 1998-2003, 2003-2008, 2008-2013, 2013-2018 and 2018-2023 is presented in Appendix 1.

CA-ANN model prediction - Model validation

LULC changes for 2033 and 2043 were predicted based on 2023 classified maps. CA-ANN model validation of the prediction maps was computed based on Kappa statistic (Table 7). The validation of prediction maps was anchored on comparing the actual LULC map for 2023 with predicted maps for 2023, 2033, and 2043. In the Kappa matrix, values of the K indices reflect the prediction estimate values. For the baseline year 2023, values of *Koverall*, *Khisto*, and *Kloc* indicate an exceedingly high threshold (>0.85). Equally, for the Percentage of Correctness (87.98%), a high value was recorded. The underlying trend for the *Koverall*, *Khisto*, and *Kloc* was quite significant, recording for 2033 and 2043 fluctuating at high intervals of 0.82 and 0.94, respectively. For the Percentage of Correctness, it also fluctuated highly within the intervals of 86.76 and 92.33. This augurs well with results from diverse findings from researchers who agree that a maximum Kappa value exceeding 0.80 is excellent (Isinkaralar and Varol, 2023). Therefore, the predicted changes could be used with high confidence levels in catchment management strategies. Based on these results, the logical conclusion on the CA-ANN model performance in predicting the trends showed an optimal output which predicted future state of LULC dynamics in Tokwe Subcatchment area.

Table 7. Model validation using Kappa indices for 2023, 2033 and 2043

K Indexes	2023	2033	2043
K Overall	0.85140	0.85535	0.86842
Khisto	0.87561	0.87206	0.84036
Kloc	0.94951	0.82810	0.87102
% of Correctness	87.98253	92.33445	86.75640

Year 2033 and 2043 LULC change prediction

The assumptions made for the predictive LULC changes are that the LULC changes are significantly influenced by projected anthropogenic factors that include increase in human population and agricultural activities. It was also assumed that existing land use policies promoting farming will continue to be in use

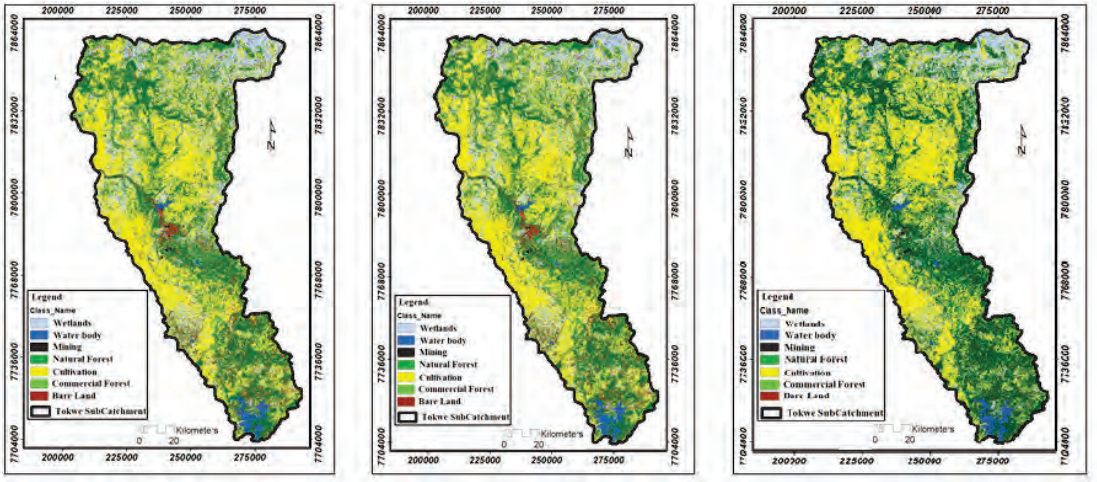


Fig. 6. (a) Predicted map 2023 (b) Predicted map 2033 (c) Predicted map 2043

www.IndianJournals.com
Not for Commercial Use
Downloaded From IP - 216.73.217.51 on dated 03-Nov-2026

Table 8. 2023, 2033 and 2043 LULC change prediction statistics

Class name	2023 Prediction (2018-2023)		2033 Prediction (2023-2033)		2043 Prediction (2033-2043)	
	Area (km^2)	Percent Change	Area (km^2)	Percent Change	Area (km^2)	Percent Change
Water body	-318.7	-18.7	-163.02	-10.4	828.66	63.4
Commercial forest	160.5	10.5	155.74	8.2	180.46	-13.8
Mining	-424.3	-42.3	-229.99	-12.1	-142.29	-10.9
Wetlands	821.0	21.0	935.79	44.1	941.00	71.2
Cultivation	826.3	26.3	917.75	48.4	976.31	74.7
Bareland	-917.4	-17.4	-175.42	-9.3	-572.42	-43.8
Natural forest	1021.5	21.5	227.94	12.0	274.50	21.0

www.IndianJournals.com
Not for Commercial Use
Downloaded From IP - 216.73.217.51 on dated 03-Nov-2026

and the implications of environmental management and conservation efforts will be constant. In the absence of the assumptions, the predicted outcomes could vary widely and may not accurately reflect future land use dynamics.

Table 8 illustrates that there was a significant shift predicted in the land use activity in Tokwe Subcatchment for 2023, the baseline year. Overall, the 2023 LULC change prediction showed declining water resources as indicated by the decrease in the water body, mining, wetlands and bareland by -18.7%, -42.3%, -21.0% and -17.4%, respectively, while commercial forest, agriculture natural forest would be on the increase by 10.5%, 26.3% and 21.5%, respectively. The water body is expected to decrease from -318.7 km^2 in 2023 to -163.02 km^2 in 2033 by -10.4%, while the wetland would increase from 821.0 km^2 in 2023 to 935.79 km^2, representing an increase of 21.0% and 44.1% in 2033. Wetlands are projected to continue to increase by 71.2% in 2043.

Based on these predicted results, bareland is predicted to decrease from -917.4 km^2 in 2023 to -175.42 km^2 in 2033, representing a drop of -17. 4% and -9.3% by 2033. A further drop in bareland is observed by 2043 to -43.8%. The findings conform to those of Maviza and Ahmed (2020) who established that bareland would continue to decline in the future. The model output and existing literature on LULC change dynamics, particularly regarding bareland, highligths the urgent need for timely and regular environmental mapping using advanced geospatial techniques to effectively capture immediate, short-term, and long-term spatiotemporal changes thereby supporting environmental sustainability and minimizing the risks of dramatic landscape shifts. The predicted changes from 2018 to 2023, 2023 to 2033 and 2033 to 2043 are indicated in figures 7, 8 and 9, respectively.

2023, 2033 and 2043 LULC prediction graphical change

In the 2018 to 2023 prediction; greatest changes in LULC are anticipated in mining, decreasing by 42.3%, while the greatest positive change is anticipated in cultivation, increasing to 26.3%. The change may indicate a shift in livelihood activities from mining to cultivation. Both wetlands and the area under water are projected to deplete by 21% and 18.7%, respectively. This could be attributed to the expansion of agricultural land or decreasing rainfall trends as established by Dzirekwa *et al*. (2023). There is a need to further research and establish what could be causing the declining water bodies to mitigate future anticipated water shortage challenges.

Between 2018 and 2023, significant changes in LULC were projected (Fig. 7). Water bodies were expected to decline by 18.7%, while commercial forests increased by 10.5%. Mining activities showed the sharpest decline at 42.3%, followed by wetlands at 21.0% and bareland at 17.4%. In contrast, cultivation expanded by 26.3%, and natural forests increased by 21.5%. The increase in wetland and reduced decline

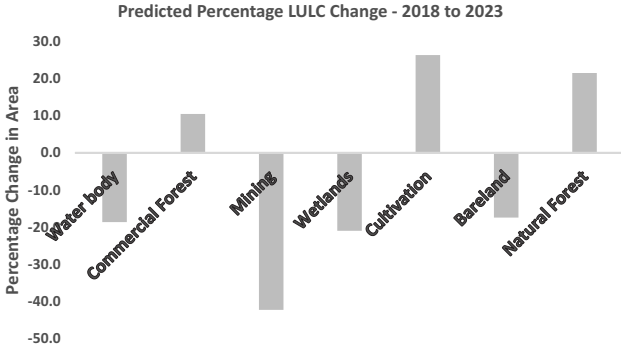


Fig. 7. Predicted LULC change from 2018 to 2023

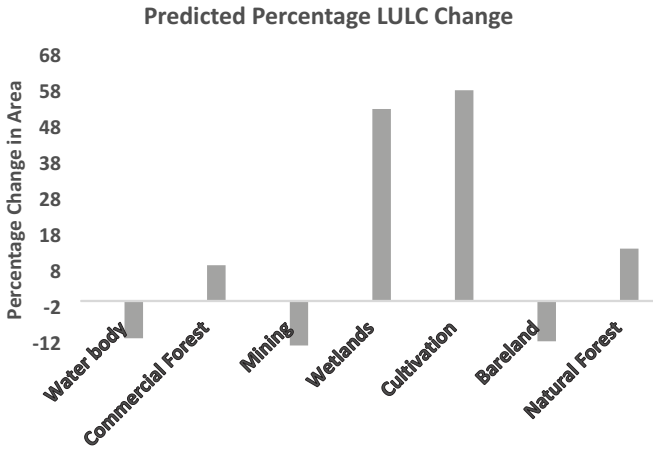


Fig. 8. Predicted LULC change from 2023 to 2033

in water body (-10.4%) may mean that there would be more water towards farming, hence the continued increase in cultivation. The projected increase in cultivation could also be attributed to anticipated population growth.

Mining activities are projected to continue declining between 2023 and 2033, with a reduction of 14.7%, while cultivation is expected to increase substantially by 58.5%. Water bodies are anticipated to decline further by 10.4%, although this represents a smaller reduction compared to the 2018-2023 period. Wetlands, however, are projected to increase significantly by 53.3%, while commercial forests are expected to grow by 9.9%. Bareland is projected to decline by 11.2%, and natural forests are anticipated to expand by 14.5%.

Overall, the findings show that LULC changes are primarily human-driven, mainly shaped by population growth, farming, and mining with consequences for soil stability and water systems.

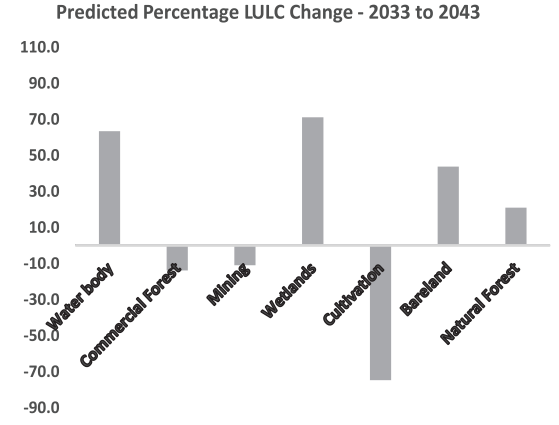


Fig. 9. Predicted LULC change 2033 to 2043

Addressing these impacts requires coordinated action by key stakeholders such as ZINWA, EMA, farmers, miners, and policymakers, to promote sustainable catchment management and safeguard water security.

LULC change validation (2023 to 2043)

A neural network learning curve as a diagnostic plot used in machine learning to visualise the performance of a model during training was generated (Fig. 10). It typically plots a performance metric (such as loss or accuracy) on the y-axis against the number of training epochs or iterations on the x-axis (Monteiro *et al,* 2016). Key components of a learning curve are a training curve and a validation curve. A training curve shows the model's performance on the training dataset. As the model learns, the training loss generally decreases, and training accuracy increases. A validation curve shows the model's performance on a separate validation dataset, which the model has not seen during training. This curve is crucial for assessing the model's ability to generalize to unseen data. For predicting 2023 baseline year, the current validation Kappa value was 0.88 and an overall accuracy of -0.00331 (Fig. 10) on the Cellular Automata Simulation, hence an excellent model prediction performance.

A neighbourhood of 3x3 pixels in magnitude size was deployed for a neural network training to consider the spatial interactions for adjacent cells based on spatial parameters of population density, slope and elevation. This culminated from adjustment of weights and biases of the neural network to minimize errors in the intervals for the observed and predicted LULC.

Limitations of the study

While this study offers a robust and data-driven analysis of LULC dynamics over a 25-year period, it is important to acknowledge certain limitations. The primary constraint of this study stems from the fact that the analysis relied solely on remote sensing and GIS-based data sources without the incorporation of conventional field-based data collection methods which may limit the validation depth for certain land cover classes. Additionally, although the use of advanced classification (SVM with RBF kernel hyper parameter tuning) and modelling techniques (MOLUSCE, CA and MLP-ANN) significantly enhanced classification accuracy and spatial prediction capabilities, the outcomes remain

www.IndianJournals.com
Not for Commercial Use
Downloaded From IP - 216.73.217.51 on dated 03-Nov-2026

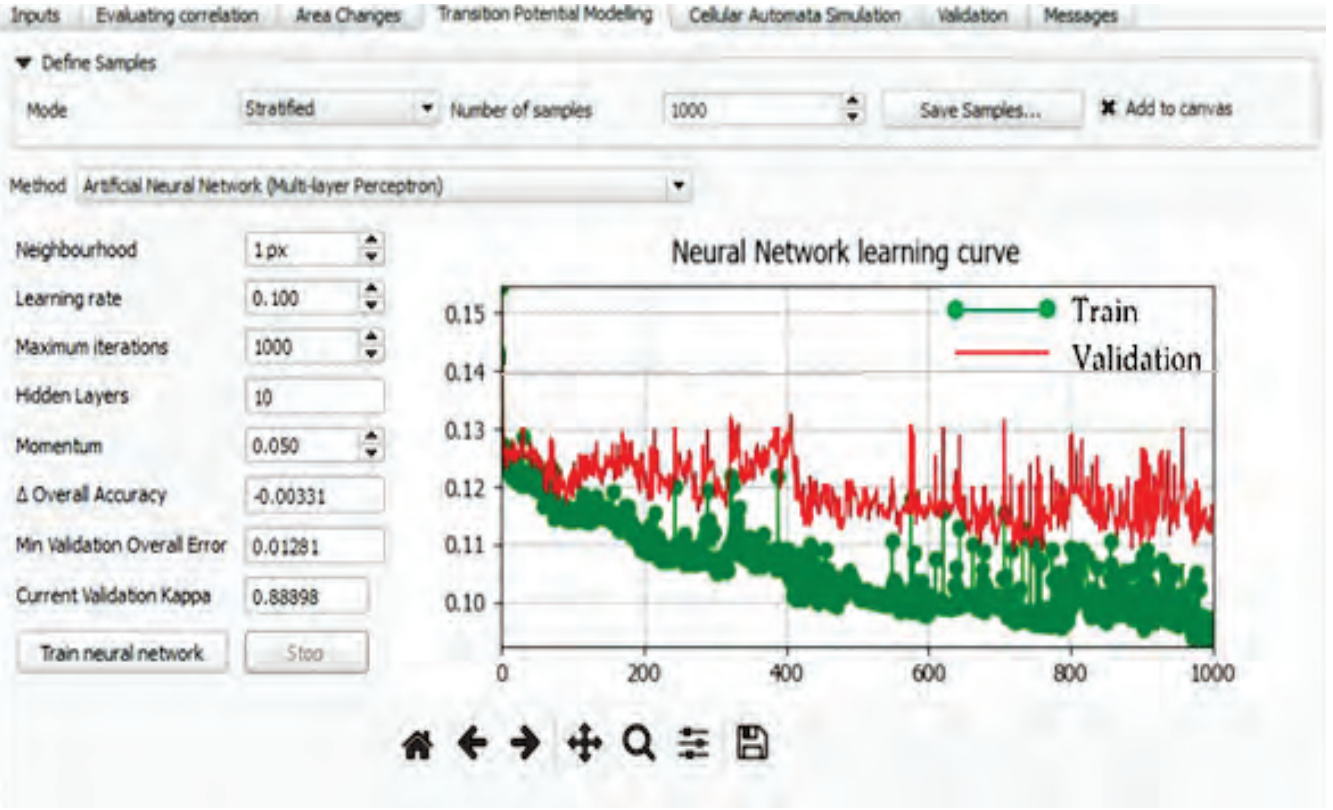


Fig. 10. Artificial Neural Network learning curve for 2023 baseline year

www.IndianJournals.com
Not for Commercial Use
Downloaded From IP - 216.73.217.51 on dated 03-Nov-2026

sensitive to model parameters and input data quality. Variations between Landsat TM and OLI sensors may also introduce minor spectral inconsistencies. Nonetheless, the integration of well-established algorithms and consistent temporal analysis ensures the study's findings are both reliable and valuable for long-term LULC monitoring and planning.

CONCLUSION

The study demonstrated that Landsat TM and OLI sensors, in combination with advanced classification and prediction techniques, facilitate a comprehensive analysis of LULC changes. The SVM classifier, enhanced through parameter tuning, achieved high accuracy, while the CA-ANN model provided reliable future predictions when integrated with essential spatial variables. This dual approach presents decision-makers with valuable insights for planning and managing land resources in the face of ongoing environmental changes.

The temporal dynamics of LULC were examined using an integrated approach of remote sensing and geographic information systems in the Tokwe Subcatchment in Zimbabwe. LULC analysis showed increased water bodies, wetlands and mining during the period 1998 to 2023. The Kappa coefficient ranged from 0.81 to 0.91 for the years 1998 to 2023, indicating perfect agreement between predicted and reference classes. The LULC prediction for 2023 and 2033 showed declining water resources (water bodies and wetland areas). This invokes the need to engage in more soil and water conservation activities to avert a reduction in water resources. Agricultural activities (commercial forest, crop cultivation and natural forest) were the only land uses projected to increase from 2023 to 2043. The change in LULC is attributed to anthropogenic factors that include increase in population and agricultural activities. Therefore, it is critical to facilitate LULC changes that promote sustainable catchment management. In addition, accurate predictions of the LULC changes facilitate pre-engagement of relevant stakeholders promoting planning and informed policy-making to address anticipated future challenges. The study contributes to the promotion of sustainable catchment management and the mitigation of future environmental degradation based on LULC changes. Future research should focus on exploring the implications of soil erosion on dam functionality and longevity, particularly in the context of changing LULC dynamics. Understanding the interplay between soil erosion and sediment accumulation in reservoirs is critical for developing strategies to mitigate

siltation and ensure sustainable water resource management. The study recommends the adoption of this methodological framework for stakeholders, which includes catchment councils, communities, Environmental Management Agency, policymakers, miners, and farmers, enabling the integration of geospatial technologies into environmental management practices for sustainable resource use and catchment resilience.

Authors' contributions

Conceptualization and designing of research work (JM, TPM); Execution of field/lab experiments and data collection (JM); Analysis of data and interpretation (JM); Preparation of manuscript (JM, TPM).

Acknowledgement

The authors acknowledge Prof Willis I. Gwenzi for intellectual assistance and technical help that included writing and editing of the manuscript.

Declaration: The authors declare that they do not have any conflict of interest.

www.IndianJournals.com
Not for Commercial Use
Downloaded From IP - 216.73.217.51 on dated 03-Nov-2026

LITERATURE CITED

Al-Rubkhi A N M, Talal A A and Mohammed A B 2017. Land use change analysis and modeling using open source (QGis)-Case Study: Boasher Willayat. Sultan Qaboos University-College of Arts and Social Science.

Anteneh M 2022. Analysis of land use/land cover change and its implication on natural resources of the Dedo watershed, Southwest Ethiopia. *The Scientific World J* **2022**(1), 6471291.

Basheer S, Wang X, Farooque A A, Nawaz R A, Liu K, Adekanmbi T and Liu S 2022. Comparison of land use land cover classifiers using different satellite imagery and machine learning techniques. *Remote Sens* **14**, 4978.

Bucała-Hrabia A 2024. Reflections on land use and land cover change under different socio-economic regimes in the Polish Western Carpathians. *Regional Environ Chang* **24**(1): 28.

Chaaban F, El Khattabi J and Darwishe H 2022. Accuracy assessment of ESA WorldCover 2020 and ESRI 2020 land cover maps for a Region in Syria. *J Geovisualization Spat Anal* **6**(2): 31.

Dey N N, Al Rakib A, Kafy A A and Raikwar V 2021. Geospatial modelling of changes in land use/land cover dynamics using Multi-layer perception Markov chain model in Rajshahi City, Bangladesh. *Environ Chall* **4**: 100148. https://doi.org/10.1016/j.envc.2021.100148

Dyson L and van Heerden J 2002. A model for the identification of tropical weather systems over South Africa. *Water SA* **28**(3): 249-58.

Dzirekwa S, Gumindoga W, Makurira H, Mhizha A and Rwasoka D T 2023. Prediction of climate change impacts on availability of surface water resources in the semi-arid Tugwi Mukosi catchment of Zimbabwe. *Sci Afr* **20**, e01691.

Foody G M 2008. Harshness in image classification accuracy assessment. *Int J Remote Sens* **29**: 3137-58.

Government of Zimbabwe 2022. Chivi District Food and Nutrition Security Profile. https://fnc.org.zw/wp-content/uploads/2023/04/Chivi-District-Profile.pdf

Government of Zimbabwe 2023. Tugwi-Mukosi combination master plan: Written statement. Ministry of Local Government and Public Works & Tugwi-Mukosi Combination Authority prepared by Zimbabwe State Universities Consortium. http://chivirdc.net/files/documents/8e63b9d1-1dd9-4ab2-bed3-8829b3865e52.pdf

Griffel E, Knapp S and van der Linden S 2020. The optimal spectral signature for land use/land cover classification of urban areas: A systematic review. *Remote Sens* **12**(15), 2415.

Guidigan M L G, Sanou C L, Ragatoa D S, Fafa C O and Mishra V N 2019. Assessing land use/land cover dynamics and its impact in Benin Republic using Land Change Model and CCI-LC products. *Earth Syst Environ* **3**: 127-37. https://doi.org/10.1007/s41748-018-0083-5

Haque M I and Basak R 2017. Land cover change detection using GIS and remote sensing techniques: A spatio-temporal study on Tanguar Haor, Sunamganj, Bangladesh. *Egypt J Remote Sens Space Sci* **20**: 251-63.

Isinkaralar O and Varol C 2023. A cellular automata-based approach for spatio-temporal modeling of the city center as a complex system: The case of Kastamonu, Türkiye. *Cities* **132**, 104073.

Kafy A A, Naim Md N H, Subramanyam G, Faisal A A, Ahmed N, Al Rakib A, Kona M and Sattar G 2021. Cellular automata approach in dynamic modelling of land cover changes using Rapid

Eye images in Dhaka, Bangladesh. *Environ Chall* **4**, 100084. https://doi.org/10.1016/j.envc.2021.100084

Li S, Song W, Fang L, Chen Y, Ghamisi P and Benediktsson J A 2019. Deep learning for hyperspectral image classification: An overview. *IEEE Trans Geosci Remote Sens* **57**(9): 6690-6709.

Malanco J A, Makurira H, Kaseke E and Gumindoga W 2018. Water management challenges at Mushandike irrigation scheme in Runde catchment, Zimbabwe. *Proc Int Assoc Hydrol Sci* **378**: 73-78.

Manatsa D and Reason C 2016. ENSO–Kalahari Desert linkages on southern Africa summer surface air temperature variability. *Int J Clim* **37**: 1728-45.

Mangi H O, Onywere S M, Kitur E C, Lalika M C and Chilagane N A 2022. Hydrological response to land use and land cover change on the slopes of Kilimanjaro and Meru Mountains. *Ecohydrol Hydrobiol* **22**: 609-26.

Maviza A and Ahmed F 2020. Analysis of past and future multi-temporal land use and land cover changes in the semi-arid Upper-Mzingwane sub-catchment in the Matabeleland south province of Zimbabwe. *Int J Remote Sens* **41**: 5206-27.

Mfwango L H, Ayenew T and Mahoo H F 2022. Impacts of climate and land use/cover changes on stream flow at Kibungo sub-catchment, Tanzania. *Heliyon* **8**: 11.

Monteiro R L, Carneiro T K G, Fontoura J R A, da Silva V L, Moret M A and Pereira H B D B 2016. A model for improving the learning curves of artificial neural networks. *PLoS One* **11**, e0149874.

Mugambiwa S S and Makhubele J C 2021. Anthropogenic flash floods and climate change in rural Zimbabwe: Impacts and options for adaptation. *Technium Soc Sci J* **21**: 809.

Munoth P and Goyal R 2020. Impacts of land use land cover change on runoff and sediment yield of Upper Tapi River Sub-Basin, India. *Int J River Basin Manag* **18**: 177-89.

Mutowo G and Chikodzi D 2013. Erosion hazard mapping in the Runde catchment: Implications for water resources management. *J Geosci Geomat* **1**: 22-28.

Ndlovu E, Prinsloo B and Le Roux T 2020. Impact of climate change and variability on traditional farming systems: Farmers' perceptions from south-west, semi-arid Zimbabwe. *Jàmbá: J Disaster Risk Studies* **12**: 1-19.

Nedd R, Light K, Owens M, James N, Johnson E and Anandhi A 2021. A synthesis of land use/land cover studies: Definitions, classification systems, meta-studies, challenges and knowledge gaps on a global landscape. *Land* **10**: 994. https://doi.org/10.3390/land10090994

Nut N, Mihara M, Jeong J, Ngo B, Sigua G, Prasad P V and Reyes M R 2021. Land use and land cover changes and its impact on soil erosion in Stung Sangkae catchment of Cambodia. *Sustain* **13**, 9276.

Ofosu G, Dittmann A, Sarpong D and Botchie D 2020. Socio-economic and environmental implications of Artisanal and Small-scale Mining (ASM) on agriculture and livelihoods. *Environ Sci Policy* **106**: 210-20.

Petropoulos G P, Knorr1 W, Scholze M, Boschetti L and Karantounias G 2010. Combining ASTER multispectral imagery analysis and support vector machines for rapid and cost-effective post-fire assessment: A case study from the Greek wildland fires of 2007. *Nat Hazards Earth Syst Sci* **10**: 305-17.

Ragini H R, Debnath M K, Gupta D S, Deb S and Ajith S 2023. Modelling and monitoring land use: Land cover change dynamics of Cooch Behar district of West Bengal using multi-temporal satellite data. *Agric Res* **12**: 387-96.

Renaud F G, Sebesvari Z and Gain A K 2021. Assessment of land/catchment use and degradation. **In**: *Handbook of water resources management: Discourses, concepts and examples*, Springer International Publishing, Cham, pp. 471-87.

Ruuska S, Hämäläinen W, Kajava S, Mughal M, Matilainen P and Mononen J 2018. Evaluation of the confusion matrix method in the validation of an automated system for measuring feeding behaviour of cattle. *Behav Process* **148**: 56-62.

Sánchez-Espinosa A and Schröder C 2019. Land use and land cover mapping in Wetlands one step closer to the ground: Sentinel-2 versus Landsat 8. *J Environ Manag* **247**: 484-98.

Seyam M M H, Haque M R and Rahman M M 2023. Identifying the land use land cover

www.IndianJournals.com
Not for Commercial Use
Downloaded From IP - 216.73.217.51 on dated 03-Nov-2026

(LULC) changes using remote sensing and GIS approach: A case study at Bhaluka in Mymensingh, Bangladesh: A case study. *Chem Environ Eng* **7**, 100293. https://www.10.1016/j.cscee.2022.100293

Shang M, Wang S X, Zhou Y and Du C 2018. Effects of training samples and classifiers on classification of landsat-8 imagery. *J Indian Soc Remote Sens* **46**(9): 1333-40.

Shukla S, Meshesha T W, Sen I S, Bol R, Bogena H and Wang J 2023. Assessing impacts of Land Use and Land Cover (LULC) change on stream flow and runoff in Rur Basin, Germany. *Sustain* **15**, 9811.

Sibanda S and Tsuyuki S 2022. Identifying the rates and drivers of spatiotemporal patterns of land use and land cover changes in the Hurungwe district, Zimbabwe: A GIS and remote sensing approach. *J Geograph Inform Sys* **14**: 652-79. https://doi.org/10.4236/jgis.2022.146037

Tonderai M, Manatsa D and Gwenzi J 2013. Environmental impacts of mining: a case of asbestos mining in Mashava, Zimbabwe. *J Sustain Dev Africa* ***15***(5): 185-96.

Wang S W, Munkhnasan L and Lee W K 2021. Land use and land cover change detection and prediction in Bhutan's high-altitude city of Thimphu, using cellular automata and Markov chain. *Environ Chall* **2**, 100017. https://doi.org/10.1016/j.envc.2020.100017

Xiao J, Watanabe T, Lu X, Chand M B, Umarhadi D A, Chen X and Avtar R 2021. Integrating land use/land cover change with change in functional zones' boundary of the East Dongting Lake National Nature Reserve, China. *Phys Chem Earth Parts A/B/C*, 103041.

Zhang M C, Zhang C, Kafy A A and Tan S 2022. Simulating the relationship between land use/cover change and urban thermal environment using machine learning algorithms in Wuhan City, China. *Land* **11**: 14.

Zhao Y, Zhang K, Fu Y and Zhang H 2012. Examining land-use/land-cover change in the Lake Dianchi Watershed of the Yunnan-Guizhou Plateau of southwest China with remote sensing and GIS techniques: 1974-2008. *Int J Environ Res Public Health* **9**: 3843-65.

Zhong B, Yang A, Jue K and Wu J 2021. Long time series high-quality and high-consistency land cover mapping based on machine learning method at Heihe river basin. *Remote Sens* **13**(8), 1596. https://doi.org/10.3390/rs13081596

www.IndianJournals.com
Not for Commercial Use
Downloaded From IP - 216.73.217.51 on dated 03-Nov-2026

APPENDIX 1

Transitional probabilities for LULC from 1998 - 2023

Transition Matrix 1998 - 2003

	WB	CF	QM	WT	CC	BL	NF	Total	Total (%)
WB	0.004	0.005	0.187	0.337	0.159	0.227	0.080	1.000	100
CF	0.061	0.040	0.022	0.205	0.070	0.111	0.491	1.000	100
QM	0.022	0.033	0.024	0.232	0.310	0.173	0.204	1.000	100
WT	0.090	0.020	0.109	0.027	0.453	0.242	0.058	1.000	100
CC	0.242	0.050	0.623	0.015	0.031	0.023	0.016	1.000	100
BL	0.007	0.393	0.006	0.001	0.580	0.006	0.008	1.000	100
NF	0.040	0.002	0.425	0.002	0.520	0.007	0.005	1.000	100

Transition Matrix 2003 - 2008

	WB	CF	QM	WT	CC	BL	NF	Total	Total (%)
WB	0.040	0.075	0.225	0.090	0.144	0.007	0.419	1.000	100
CF	0.002	0.403	0.084	0.020	0.049	0.393	0.050	1.000	100
QM	0.065	0.322	0.245	0.106	0.187	0.006	0.069	1.000	100
WT	0.002	0.255	0.362	0.028	0.337	0.001	0.015	1.000	100
CC	0.002	0.079	0.675	0.013	0.199	0.000	0.031	1.000	100
BL	0.009	0.316	0.177	0.242	0.227	0.006	0.023	1.000	100
NF	0.005	0.691	0.134	0.058	0.089	0.008	0.016	1.000	100

Transition Matrix 2008 - 2013

	WB	CF	QM	WT	CC	BL	NF	Total	Total (%)
WB	0.419	0.007	0.040	0.144	0.225	0.090	0.075	1.000	100
CF	0.050	0.393	0.002	0.049	0.084	0.020	0.403	1.000	100
QM	0.069	0.006	0.065	0.187	0.245	0.106	0.322	1.000	100
W	0.015	0.001	0.002	0.337	0.362	0.028	0.255	1.000	100
CC	0.031	0.000	0.002	0.199	0.675	0.013	0.079	1.000	100
BL	0.023	0.006	0.009	0.227	0.177	0.242	0.316	1.000	100
NF	0.016	0.008	0.005	0.089	0.134	0.058	0.691	1.000	100

Transition Matrix 2013 - 2018

	WB	CF	QM	WT	CC	BL	NF	Total	Total (%)
WB	0.028	0.355	0.009	0.015	0.386	0.006	0.200	1.000	100
CF	0.013	0.029	0.505	0.031	0.337	0.001	0.084	1.000	100
QM	0.240	0.010	0.039	0.020	0.190	0.030	0.470	1.000	100
W	0.048	0.601	0.002	0.016	0.223	0.006	0.105	1.000	100
CC	0.060	0.075	0.215	0.419	0.089	0.008	0.134	1.000	100
BL	0.020	0.403	0.102	0.050	0.214	0.006	0.205	1.000	100
NF	0.106	0.322	0.002	0.069	0.048	0.390	0.062	1.000	100

Transition Matrix 2018 - 2023

	WB	CF	QM	WT	CC	BL	NF	Total	Total (%)
WB	0.718	0.008	0.055	0.006	0.039	0.083	0.092	1.000	100
CF	0.012	0.196	0.004	0.089	0.162	0.042	0.496	1.000	100
QM	0.026	0.018	0.009	0.106	0.165	0.063	0.611	1.000	100
WT	0.101	0.010	0.217	0.098	0.281	0.111	0.183	1.000	100
CC	0.010	0.023	0.006	0.410	0.346	0.034	0.171	1.000	100
BL	0.011	0.010	0.007	0.228	0.583	0.028	0.133	1.000	100
NF	0.122	0.130	0.202	0.004	0.406	0.130	0.006	1.000	100

www.IndianJournals.com
Not for Commercial Use
Downloaded From IP - 216.73.217.51 on dated 03-Nov-2026